Heat Capacities and Phase Transitions of Crystalline 1,3,5-Trichloro-2,4,6-trimethylbenzene†

Takahiro FUJIWARA, Tooru ATAKE,†† and Hideaki CHIHARA*
Department of Chemistry and Microcalorimetry Research Center, Faculty of Science, Osaka University, Toyonaka, Osaka 560
††Research Laboratory of Engineering Materials, Tokyo Institute of Technology, 4259 Nagatsuta-cho, Midori-ku, Yokohama 227
(Received September 7, 1989)

Heat capacities were measured of 1,3,5-trichloro-2,4,6-trimethylbenzene by adiabatic calorimetry from 3 to 327 K covering the three stable solid phases, II, III, and IV. The phase transitions, III–II and IV–III, are of first order and accompanied by a hysteresis effect. The IV–III transition occurs at 163.5 K when the crystal cooled slowly from Phase II, whereas the heat capacity anomaly splits into two at 158.7 and 163.5 K if the crystal was cooled rapidly. From the time dependence of Raman spectra at low frequencies, kinetics of transition II–III was studied; it is best explained by diffusionless nucleation mechanism. The thermal hysteresis can be rationalized by assuming the existence of a metastable phase IV′.

There are a series of interesting crystals between hexamethylbenzene and hexachlorobenzene produced by successive replacement of chlorine atoms with methyl groups. Whereas a methyl group and a chlorine atom have very similar van der Waals radii (0.177 and 0.178 nm, respectively), the properties of crystals are not simply dependent on the size of the substituents; the interaction between methyl groups has not been fully understood.

In our previous studies on hexamethylbenzene,[1] it has been elucidated that the phase transition at 117 K was not a second order transition as had been believed[2] but it was of a first order superimposed by a broad anomaly in the heat capacity related to coupled internal rotation of methyl groups. NMR studies confirmed such coupling of methyl rotation[3] from the field-cycling experiments. The calorimetric investigation also revealed an interesting hysteresis phenomenon.[4] Fully deuterated hexamethylbenzene, $C_6(CD_6)_6$, showed almost twice as large an enthalpy of transition between phase III and phase II as its hydrogen analogue $C_6(CH_3)_6$.[5] Thus, the behavior of methyl groups in hexamethylbenzene turned out to be far more complicated than one would think. It was then considered that if the methyl groups are decoupled by alternate replacement with chlorine atoms, we would see a simplified version of methyl group interaction and motion.

We measured heat capacities of 1,3,5-trichloro-2,4,6-trimethylbenzene (hereafter referred to as TCTMB) with particular attention to phase relations and hysteresis effects, proton spin-lattice relaxation time, and Raman spectra over a wide range of temperature. The NMR part of the studies has been published elsewhere.[6] The crystal structure was determined at room temperature in phase III;[7] its space group is $P\bar{1}$ with two molecules in a unit cell of a=0.8866 nm, b=0.8905 nm, c=0.7767 nm, α=113.59°, β=107.10°, and γ=59.63°. The molecules are stacked in a tilted column in an antiferroelectric manner, i.e. a chlorine atom of a molecule comes on top of a methyl group of the neighboring molecule. Structure in other phases is not known.

† Contribution No. 16 from Microcalorimetry Research Center, Faculty of Science, Osaka University.

Experimental

A sample of 1,3,5-trichloro-2,4,6-trimethylbenzene (TCTMB) was synthesized by chlorination of 1,3,5-trimethylbenzene (mesitylene). Mesitylene and carbon tetrachloride were purchased from Wako Pure Chemicals Industries, Ltd. Gaseous chlorine was bubbled into a mixture of mesitylene and carbon tetrachloride cooled by ice-water while stirring. TCTMB precipitated, which was recrystallized several times from hot ethanol: Found: C, 48.36; H, 4.04; Cl, 47.38%, Calcd: C,48.36; H, 4.06; Cl, 47.58%. The gas chromatography and high resolution NMR (90 MHz) of the sample were consistent with the target product. It was further purified by sublimation in vacuo at 45 °C. The final purity of sample was better than 99.9 moles percent by gas chromatography.

The sublimed specimen was melted at 210 °C in dry helium gas, cooled slowly to room temperature, pulverized, and used for calorimetry. The mass of the specimen used for heat capacity measurements was 14.2973 g (0.0639614 mol). Its heat capacity contributed about 64% to the total heat capacity at 10 K, about 41% at 150 K, and about 48% at 300 K. A small amount of helium gas (5.3 kPa at 27 °C) was used for heat exchange inside the calorimeter vessel and its contribution to the total heat capacity was safely ignored.

The adiabatic calorimeter assembly and thermometers used for the measurements were the same as described previously.[8] A platinum resistance thermometer (Model 8164, Leeds & Northrup Co.), calibrated on the IPTS-68, was used above 13.81 K and a germanium resistance thermometer (CryoCal Inc.) was used below 14 K. The resistance of the thermometers was measured with a thermometer bridge (Leeds & Northrup, Model 8079 type ER). The temperature scales were described elsewhere.[8] The calorimeter vessel was made of gold-plated copper with an inside volume of about 31 cm³.

For the DTA measurements, a specimen was sealed in a glass tube with helium gas at 6 kPa (room temperature) for thermal exchange.

The Raman spectra were recorded on JASCO Model R800 spectrophotometer at 514.5 nm, 220 mW with an Ar ion laser between 5 and 80 cm^{-1} and between 78 and 320 K. The powdered specimen was loaded in a glass capillary tube with helium gas at 10 kPa for heat exchange.

Results

Differential Thermal Analysis (DTA). Prior to the heat capasity measurements, DTA measurements were made. On heating the specimen, which had been cooled to 88 K, four endothermic peaks were observed approximately at 160 K (a), 314 K (b), 401 K (c), and 485 K (d). In the cooling direction, on the other hand, the anomaly corresponding to the anomaly a was not observed but the other three exothermic peaks were observed at about 281 K, about 399 K, and about 474 K, respectively.

The peak d at 485 K is the melting transition, the largest of the four. The one at 401 K (c) is a lambda-shaped peak, whereas the transitions a and b are the first order solid–solid transitions. No additional anomalies were found by heat capacity measurements. Altogether there are four phases in the solid state of TCTMB. We denote the phases I, II, III, and IV from the melting point downwards.

Heat Capacity. Measured heat capacities of TCTMB between 3 to 327 K are given in Table 1 and a portion of the data are shown in Fig. 1 covering only the lower two phase transitions. As the anomaly around 160 K shows a complicated feature depending on the sample history and it is also related to the transition at 314 K as described later, two representative runs are shown. The difference between the two runs is whether the sample has experienced the transition at 314 K or not, that is, the lower temperature peak corresponds to the "virgin" sample and the higher one corresponds to the sample once heated above the transition at 314 K. We denote the virgin sample by A, and the one once heated above 314 K in the calorimeter by B. As the discussion in the following will give certain evidence, Sample A is considered to be in the non-equilibrium state, whereas Sample B is considered to represent the equilibrium state.

III–IV Transition. Sample A was cooled down to 132 K, subjected to several cycles of the III–IV transition region, and then cooled down again to 100 K, where the specimen was brought to phase IV. After heating it up to 144 K, the heat capacity measurement was started, waiting as long as 2 hours after every heat input for equilibrium.

The result is shown in Fig. 2, where splitting of the anomaly into two peaks is seen at 158.7 and 163.5 K.

On the other hand, if we waited only about 30 min after a heat input, only a single peak resulted at 158.7 K. Since this fact was considered to show that the specimen was in a non-equilibrium state, the effect of annealing was studied. Thus, the sample A was cooled from room temperature to 100 K and then heated to 161 K, an intermediate temperature between the two

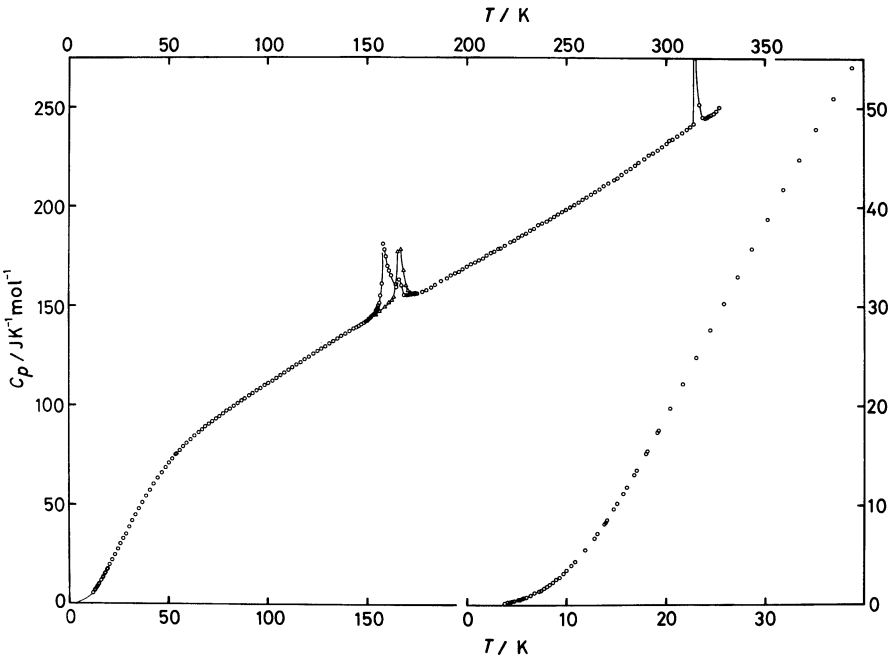

Fig. 1. Molar heat capacities of 1,3,5-trichloro-2,4,6-trimethylbenzene between 3 and 327 K. Sample A (○) and Sample B (△) differ only in the transition region at about 160 K; therefore only data of Sample A are plotted except in the transition region.

Table 1. Measured Molar Heat Capacities of 1,3,5-Trichloro-2,4,6-trimethylbenzene. Relative Molar Mass=223.53

T	C_p	T	C_p	T	C_p
K	J K^{-1} mol^{-1}	K	J K^{-1} mol^{-1}	K	J K^{-1} mol^{-1}
Series 1		158.092	147.21	245.679	196.01
54.287	75.713	159.981	147.56	247.674	197.24
55.946	77.495	161.878	147.90	249.695	198.35
57.645	79.313	163.816	148.90	251.743	199.58
59.366	81.010	165.770	149.97	253.782	200.76
61.260	82.767	167.737	151.04	255.811	202.13
63.296	84.675	169.785	152.18	257.833	203.38
65.264	86.308	171.882	153.24	259.905	204.51
67.081	87.798	173.959	154.53	262.027	205.99
68.846	89.270	176.017	155.72	264.139	207.22
70.658	90.683	178.058	156.93	266.282	208.62
72.455	92.061	180.083	158.17	268.514	210.31
74.267	93.342	182.093	159.31	270.787	211.71
76.067	94.650	184.086	160.55	273.058	215.07
77.857	95.945	187.053	162.39	275.306	214.44
79.641	97.186	189.974	163.83	277.549	216.03
81.407	98.450	191.919	165.10	279.781	217.57
83.310	99.775	193.876	166.29	282.002	219.03
85.330	101.14	195.883	166.92	284.211	220.54
87.311	102.50	197.938	168.38	286.469	222.12
88.944	103.61	199.982	169.72	288.770	223.97
90.926	104.96	202.014	171.00	291.058	225.77
92.907	106.25	203.957	171.83	293.336	226.87
94.890	107.58	205.945	172.86	295.603	228.26
96.839	108.87	207.928	173.77	297.859	230.00
98.792	110.13	209.901	175.17	300.105	231.81
100.749	111.31	211.898	176.48	302.340	233.32
102.759	112.58	214.405	177.75		
104.822	113.94	216.897	179.05	Series 4	
106.857	115.28	218.893	180.28	12.048	5.434
108.866	116.61	220.879	181.50	13.094	7.174
110.852	117.88	222.889	182.63	14.072	8.687
112.813	119.10	224.927	183.67	15.034	10.226
114.842	120.46	226.957	184.87	16.011	11.836
116.927	121.72	228.977	186.07	17.003	13.550
118.978	123.32	231.025	187.48	18.065	15.451
121.003	124.45	233.098	188.77	19.183	17.543
123.215	125.88	235.200	189.75	20.345	19.761
125.406	127.08	237.332	191.08	21.612	22.190
127.364	128.47	239.450	192.34		
129.305	129.71	241.560	193.60	Series 5	
131.233	131.02	243.696	194.66	12.799	6.725
133.204	132.17	241.545	193.49	13.759	8.198
135.225	133.52	243.847	195.08	14.697	9.653
137.229	134.86	246.123	196.50	15.644	11.202
139.215	136.01			16.769	13.102
141.186	137.37	Series 3		17.952	15.223
143.142	138.59	213.579	177.18	19.091	17.372
145.083	139.98	215.586	178.58	20.320	19.709
147.007	141.36	217.584	179.49	21.590	22.160
148.981	142.71	219.572	180.76	22.951	24.837
151.003	143.90	221.550	181.96	24.353	27.589
153.009	146.08	223.556	182.94	25.724	30.259
154.993	149.00	225.587	184.09	27.115	32.960
156.932	158.50	227.607	185.37	28.575	35.728
158.879	165.51	229.620	186.41	30.167	38.746
160.882	158.89	231.622	187.72	31.769	41.766
162.751	157.36	233.615	188.84	33.386	44.754
		235.633	190.75	35.112	47.823
Series 2		237.679	191.42	36.912	50.993
152.565	142.24	239.639	192.42	38.808	54.154
154.274	143.40	241.663	193.68	40.764	57.347
156.181	144.83	243.675	194.69	42.723	60.403

Table 1. (Continued)

T	C_p	T	C_p	T	C_p
K	J K^{-1} mol^{-1}	K	J K^{-1} mol^{-1}	K	J K^{-1} mol^{-1}
44.691	63.337	159.394	174.81	6.782	1.122
46.661	66.128	160.133	169.93	7.227	1.344
48.554	68.743	160.992	167.62	7.730	1.644
50.351	71.093	161.913	165.13	8.306	2.025
52.095	73.220	162.837	163.58		
53.824	75.289	163.765	160.78	Series 12	
		164.807	164.27	3.769	0.1805
Series 6		165.961	163.15	4.102	0.2428
143.227	137.74	167.177	159.98	4.468	0.3151
145.314	139.19	168.461	155.40	4.882	0.4215
147.381	140.52	169.751	155.14	5.292	0.5464
149.431	141.85	171.037	155.42	5.700	0.6766
151.463	143.33	172.374	155.45	6.100	0.8289
153.474	145.12	173.767	155.45	6.500	0.9836
155.465	148.12	175.160	156.06		
157.475	157.73	176.549	156.70	Series 13	
159.486	168.17	177.932	157.22	4.151	0.2437
161.481	160.60	179.369	158.07	4.518	0.3349
163.504	156.14			4.901	0.4273
165.537	154.14	Series 9		5.300	0.5448
167.561	153.32	151.787	143.37	5.958	0.7745
169.591	153.63	153.778	144.98	6.372	0.9405
171.554	154.13	155.749	147.28	6.813	1.135
173.449	155.01	157.682	156.56	7.295	1.382
175.334	155.90	159.565	163.66	7.844	1.706
177.269	156.97	161.437	157.63	8.395	2.087
179.248	157.90	163.304	164.17	9.004	2.545
181.218	159.17	164.746	164.33	9.720	3.177
183.178	160.37	165.785	161.66	10.487	3.945
185.184	161.53	166.891	158.03		
		168.060	157.51	Series 14	
Series 7		169.247	156.03	7.431	1.442
157.777	144.96	170.494	155.00	8.043	1.845
159.252	145.97			8.653	2.264
160.719	146.88	Series 10		9.304	2.770
162.180	147.78	149.694	141.97	10.018	3.477
163.633	148.62	151.698	143.59	10.869	4.372
165.079	149.52	153.314	144.67	11.843	5.525
166.520	150.20	154.547	146.08	12.863	6.790
167.953	150.95	155.831	148.06	13.918	8.312
169.380	151.72	157.163	151.56		
		158.174	164.93	Series 15	
Series 8		158.865	168.96	9.256	2.775
144.795	139.04	159.554	167.31	10.037	3.504
145.755	139.77	160.245	165.89	10.914	4.426
146.646	140.32	160.999	161.06	11.877	5.556
147.534	140.75	161.875	159.88	12.918	6.882
148.420	141.36	162.804	164.21	14.026	8.545
149.303	142.07	163.724	165.82	15.131	10.743
150.119	142.35	164.699	165.77		
150.870	143.34	165.909	161.66	Series 16	
151.618	144.04	167.302	159.05	147.173	140.27
152.364	144.98	168.759	157.08	149.360	141.69
153.107	145.69	170.394	156.63	151.522	143.27
153.786	146.09			153.661	145.10
154.340	147.53	Series 11		155.769	148.41
154.769	148.16	3.612	0.1520	157.805	166.83
155.136	148.90	3.661	0.1624	159.774	168.79
155.561	150.14	4.309	0.2896	161.814	158.05
156.106	151.55	4.758	0.3896	163.946	153.85
156.707	155.13	5.190	0.5126	166.084	152.82
157.359	161.19	5.599	0.6480	168.150	153.36
158.047	181.05	5.988	0.7882	170.204	153.15
158.718	178.24	6.377	0.9420	172.307	154.11

Table 1. (Continued)

T	C_p	T	C_p	T	C_p
K	J K^{-1} mol^{-1}	K	J K^{-1} mol^{-1}	K	J K^{-1} mol^{-1}
174.402	155.31	174.667	156.35	Series 23	
176.649	156.39	177.005	156.98	310.197	238.94
		179.332	158.02	311.969	240.32
Series 17		181.645	159.21	313.733	241.75
297.966	230.18			314.823	1109.89
300.599	232.39	Series 19		315.018	341.98
303.110	233.75	310.140	239.13	316.590	251.47
305.489	235.52	312.095	240.48	318.204	245.04
307.795	237.19	313.680	241.90	319.588	244.49
310.150	239.14	315.253	243.38	320.568	245.16
312.538	241.19	319.402	528.14	321.488	245.58
314.898	242.64	323.542	251.24	322.579	246.21
319.203	275.84	325.085	248.73	323.839	247.03
321.593	262.50	326.624	249.78	325.210	248.16
324.017	250.48			326.519	250.10
326.458	250.39	Series 20			
		152.029	143.65	Series 24	
Series 18		154.486	145.55	308.999	238.55
82.787	99.604	156.760	147.14	310.859	239.95
84.813	100.99	158.851	149.26	312.770	242.21
86.881	102.38	160.922	151.70	314.667	245.40
88.990	103.80	162.390	152.65	316.527	258.84
91.137	105.24	163.266	154.27	317.782	1403.85
93.232	106.63	164.273	160.79	318.720	349.68
95.284	107.98	165.524	177.10	320.189	257.18
97.384	109.35	166.884	178.27	321.328	245.62
99.452	110.70	168.258	167.65	322.382	246.17
101.523	111.95	169.518	160.24	323.547	246.71
103.601	113.27	170.652	157.61	324.712	247.58
105.728	114.69	171.860	156.38	325.873	248.49
107.905	116.10	173.142	155.90		
110.044	117.61	174.491	156.05	Series 25	
112.163	118.96	175.909	156.25	307.463	236.91
114.331	120.39	177.674	157.02	309.394	238.27
116.586	121.79	179.643	157.89	311.370	239.64
118.852	123.36			313.404	240.86
121.129	124.74	Series 21		315.432	241.75
123.495	126.20	151.350	141.36	317.516	243.81
125.909	127.67	153.397	142.55	319.652	244.52
128.370	129.20	155.428	143.76	321.840	245.72
130.874	130.75	157.444	144.94	324.079	246.84
133.323	132.31	159.445	146.28		
135.738	133.67	161.434	147.37		
138.193	135.37	163.410	148.49		
140.625	136.90	165.372	149.65		
142.999	138.28	167.323	150.71		
145.363	140.01				
147.749	141.41	Series 22			
150.155	143.05	148.302	141.39		
152.631	144.82	150.528	142.94		
155.133	146.94	152.822	144.47		
157.689	149.57	155.269	146.33		
159.974	151.90	157.864	148.90		
161.908	155.30	160.511	152.11		
163.658	159.57	163.197	158.05		
165.141	167.51	165.784	177.80		
166.449	169.62	171.431	161.68		
167.687	160.62	176.802	156.71		
168.941	158.21	178.760	157.65		
170.354	156.68	180.789	158.80		
172.317	156.02				

peaks, where it was annealed for 15 h. The measurements, made after cooling it down to 100 K again, still showed split peaks with a larger high-temperature peak; therefore, the peak at 163.5 K grows as a result of annealing. A longer annealing time at 161 K did not make any difference.

In the case of Sample B, a single peak of transition anomaly was observed at 166.4±0.5 K in the heating direction when it had been cooled down to 88 K prior to the commencement of measurement. It was interesting to note that in Sample B the transition temperature depends on the "reverse" temperature T_{rev}, i.e. the lowest temperature to which the sample was cooled within the region of Phase IV, and that the lower the reverse temrerature, the higher the transition temperature. Once the crystal has become Sample B, i.e. once it has been heated above the II–III transition, it does not revert to Sample A. In other words, Sample B always shows a single peak around 165 K, the temperature of the anomaly depending on the immediate past thermal history.

The enthalpy of transition IV→III also depends on the thermal history. Table 2 shows the enthalpies and the transition temperatures for Samples A and B measured from different reverse temperature T_{rev}. Note, however, that there is a considerable amount of uncertainty in ΔH_t which comes from difficulty of evaluating the "normal" part of heat capacity. Table 2 shows that (1) ΔH_t is larger when T_{rev} is lower and (2) in the case of Sample B the transition temperature is significantly higher when T_{rev} is below 100 K and ΔH_t is correspondingly larger.

II-III Transition. The heat capacity anomaly at this transition point is associated with a superheating effect. The point a of Fig. 3, which is a cumulative enthalpy in III–II transition region, corresponds to an apparent equilibrium state; the calorimeter reaches a steady temperature 20 min after heating was turned off. At the point b, a slow cooling drift persisted which was thought of as the beginning of the phase

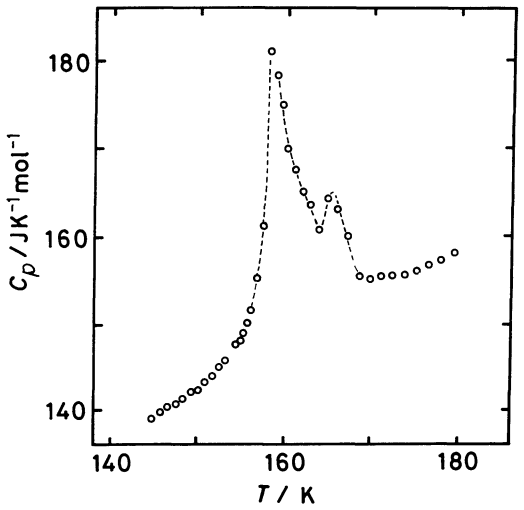

Fig. 2. Heat capacities of Sample A in the IV–III transition region.

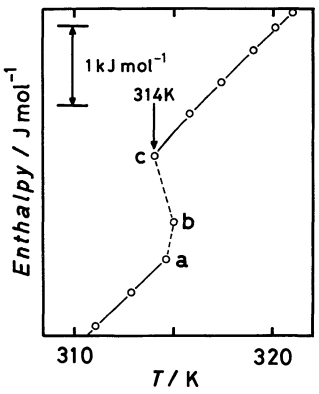

Fig. 3. Cumulative enthalpy in the III–II transition region. Points a and b correspond to superheated states.

Table 2. Enthalpy of Transition IV → III[a)]

T_t/K	T_t'/K	ΔH_t/kJ mol^{-1}	T_{rev}/K	Remark
Sample A				
158.8±0.3	—	0.142	147	a
158.8±0.4	164.1±0.5	0.150	142	b
158.4±0.2	—	0.237	100	a
159.0±0.3	163.5±0.5	0.158	109	c
158.9±0.3	163.6±0.5	0.184	109	d
Sample B				
163.6±0.2		0.087	128	
163.5±0.2		0.099	120	
165.9±0.2		0.121	82	
166.4±0.2		0.140	80	
166.5±0.1		0.174	77	

a) T_t is the lower transition temperatures and T_t' is the upper transition temperature of split peaks. T_{rev} is the temperature to which the specimen was cooled before measurements. a: "Quick" measurement waiting for 30 min after heat input. b: "Slow" equilibrium measurement. c: Annealed at 161 K for 15 h and measured from 151 K. d: Annealed at 161 K for 40.5 h and measured from 149 K.

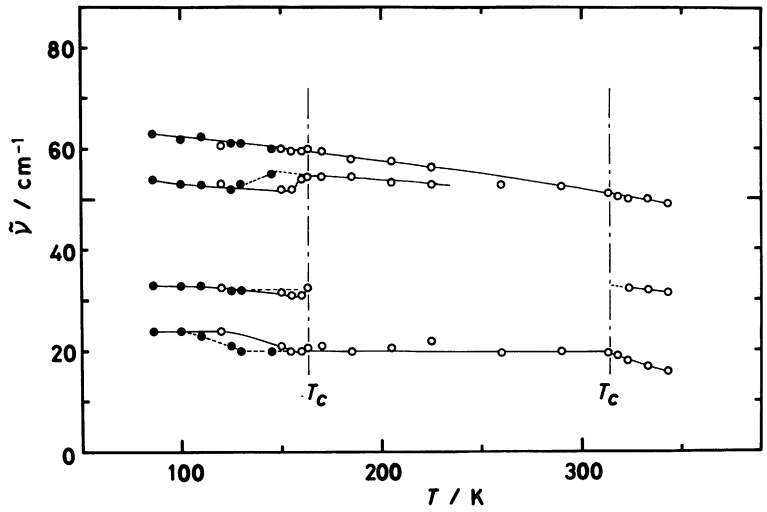

Fig. 4. Temperature dependence of Raman frequencies of Sample B in the lattice mode region; heating direction (○) and cooling direction (●).

transition. Another heat input is done after b; the temperature then dropped (point c) by about 0.4 K and reached a steady state (±0.002 K min^{-1}) after about 40 h under adiabatic conditions. Such observation indicates that the transition is of the first order and that it occurs very slowly by thermal stimulation. The equilibrium transition point in the heating direction is tentatively defined as 314 K for the sample which was cooled to 211 K prior to the measurement.

The enthalpy of transition as well as the temperature of the transition depends on the reverse temperature T_{rev}, the temperature to which the sample was cooled; the lower the reverse temperature, the larger the enthalpy of transition. This observation is very similar to that for the IV→III transition.

Raman Spectra. Temperature dependence of Raman spectra in the lattice mode region in Phases II, III, and IV is shown in Fig. 4. There is no difference between Sample A and Sample B except that a weak shoulder at about 60 cm^{-1} becomes even weaker in Sample A as it is cooled in Phase IV. In Phase III, a band at about 33 cm^{-1} is missing which exists in Phase II. The temperature coefficient of the Raman frequencies shows differences among the phases: The band at 60 cm^{-1}, which is seen only in Sample B has a constant downward slope (Fig. 4) whereas the band at 20 cm^{-1} has a break at each transition point. Because the potential barrier hindering the internal rotation is only 2.4 kJ mol^{-1} high in Phase IV with a correspondingly small tunneling frequency of 830 MHz,[6] the Raman bands probably originate from translational and rotational modes.

Kinetics of Transition, II→III. Figure 5 shows the change of Raman spectrum with time of Sample B which was undercooled from Phase II and kept at 292 K. The band at 33 cm^{-1} gradually decreases its intensity in about 5 h. Its integrated intensity, normalized in reference to the intensity of the band at 55 cm^{-1}, was taken as a measure of the fraction y of the specimen that had been transformed to Phase III (Fig. 6). Figure 6 is typical rate behavior for a homogeneous nucleation/growth mechanism in the solid state,

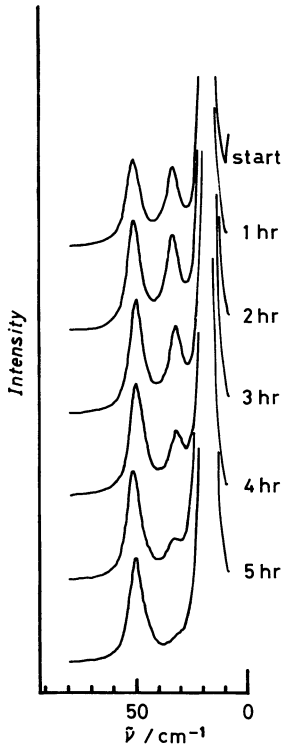

Fig. 5. Intensity of Raman bands as a function of time at 292 K. Disappearance of the band at 33 cm^{-1} shows progress of the II–III transition.

$$y = 1 - \exp[-(kt)^n], \quad (1)$$

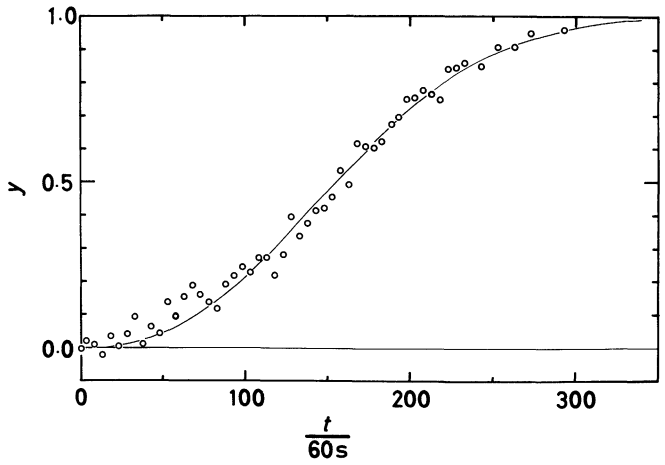

Fig. 6. Avrami plot of the fraction y which was transformed from Phase II to Phase III as a function of time t, corresponding to the change in Fig. 5. Solid line represents Eq. 1.

which is known as Avrami or Johnson-Mehl[9] equation. Here k is the reciprocal of the "growth time" and n is an exponent which depends on the model. Fitting of Eq. 1 to the experimental data for $t>79$ s gave $n=2.4$ and $k=5.5\times10^{-3}$ s^{-1}; the parameters well reproduce the experimental results as shown by the solid curve in Fig. 6. The value of the exponent n is close to that of the model of diffusionless transition in which nucleation of the new phase occurs at the beginning and continues at grain edges at later times.[10]

Discussion

The phase behavior of TCTMB is very complicated because certain properties of the phase transitions studied here are dependent both on temperature and on time in addition to the thermal history of the specimen. In order to establish a reasonable model of the phase relationship, we begin by summarizing experimental results with particular attention to the time effect, temperature effect, and thermal history.

The II-III Transition: (1) The transition from Phase II to Phase III is a sluggish one. Phase II is easily undercooled down to 293 K and while maintaining the specimen at 292 K, it takes at least about 5 h for the transition II→III to complete (as far as the sensitivity of Raman spectroscopy permits the detection of Phase III). In the heating direction, the transition III→II also proceeds very slowly; it took about 40 h in the calorimeter at 314 K.

(2) Single crystals were grown at 298 K from a benzene solution, which we believe existed in Phase II because the phase usually undercools down to 293 K. Such a single crystal undergoes a deformation characteristic to a Martensitic transition by applying a small external stress[10] (see Fig. 7). Apparently, the deformation was accompanied by the transition from Phase II to Phase III.

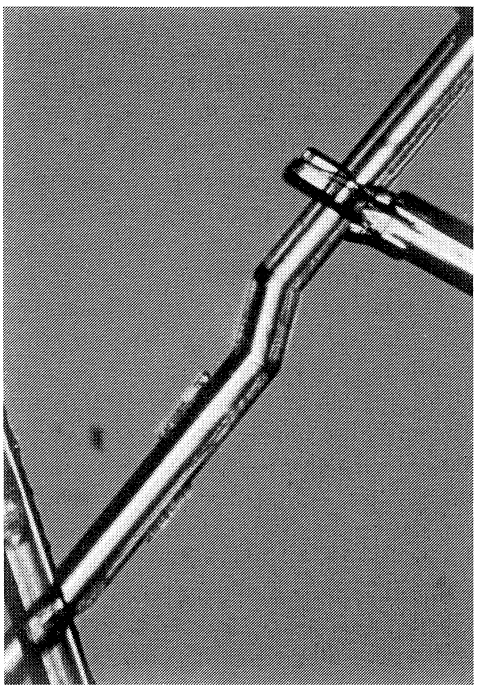

Fig. 7. Microscope photograph showing a stress-induced transition of Martensite type in 1,3,5-trichloro-2,4,6-trimethylbenzene. A single crystal shows characteristic deformation by application of an external stress.

(3) The enthalpy of III–II transition depends on the temperature to which the specimen had been cooled prior to the heat capacity measurements. The lower the temperature, the larger the enthalpy. However, the heat capacity anomaly at the III–II transition always showed a single peak.

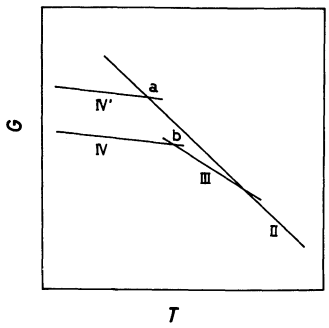

Fig. 8. Proposed Gibbs energy diagram for 1,3,5-trichloro-2,4,6-trimethylbenzene. Point a corresponds to a transition, metastable-supercooled states.

The III-IV Transition: (4) Sample A showed split peaks in the heat capacity curve whereas Sample B always showed a single peak. Sample B does not revert to Sample A.

(5) Annealing Sample A at a temperature between the two peaks has some effect of enhancing the higher peak but the split peak feature persists. If measured quickly, only one anomaly at 158.7 K is seen in Sample A.

(6) The enthalpy of transition is larger when T_{rev} is lower for both Sample A and Sample B. The temperature of transition is higher when T_{rev} is lower in the case of Sample B but it is not the case for Sample A.

Let's now assume that Sample B in Phase III represents the thermodynamic equilibrium state; this assumption is considered to be a plausible hypothesis in view of (1). If Phase II is cooled rapidly into the Phase III region as in the preparation of Sample A, the specimen will become a mixture of Phase III and undercooled Phase II because of (1). A working Gibbs energy will then be something like Fig. 8 where Sample A at the lowest temperature consists of Phases IV' and IV and Sample B is purely in Phase IV.

The split peaks of Sample A (4) are the manifestation of the transitions at points a and b of Fig. 8. Because the enthalpy change at point a must be larger than that at point b, it is understood that the enthalpy of transition is larger in Sample A than that for Sample B (Table 2). There is an effect of T_{rev} only on the transition at point b and not on the transition at point a; this is probably because there can hardly be a reproducible hysteresis effect between metastable phases. It is inferred that there is a large hysteresis loop associated with the transition at b, i.e. the III–IV transition. Thus, when Phase III is cooled through the point b, it is transformed progressively but slowly into Phase IV as the temperature is lowered. This can explain (6).

While such a working model can explain, by and large, all the major experimental observation, it is difficult to rationalize the effect of annealing (5). It may be that stabilization of undercooled Phase II is also a slow kinetic process having a strong temperature dependence of the rate of stabilization.

The hysteresis effect and split anomalies in the heat capacity curve observed in TCTMB appear to be similar to the corresponding effects in hexamethylbenzens but their origin is quite different. The occurrence of split peaks in the heat capacity is related to the thermal hysteresis in either crystal: However, it is due to a "memory" effect in the case of hexamethylbenzene, whereas it is inferred to be due to two separate transitions in the case of TCTMB. Such a difference is probably related to a difference in the intermethyl interaction; there is a coupled, collective mode in the methyl reorientation in HMB in contrast to independent stochastic reorientation in TCTMB. A very small activation energy (2.4 kJ mol^{-1})[6] for methyl rotation in TCTMB as compared to that in HMB (8.0 kJ mol^{-1}) supports this idea. This also means that methyl–methyl interaction between neighbor molecules has a comparable magnitude to the interaction within the same molecule and is relatively more important in TCTMB.

This work was supported by the Grant-in-Aid (No. 58470013) for Scientific Research from the Ministry of Education, Science and Culture.

References

1) T. Atake, H. Gyoten, and H. Chihara, *J. Chem. Phys.*, **76**, 5535 (1982).
2) M. Frankosky and J. G. Aston, *J. Phys. Chem.*, **69**, 3126 (1965).
3) S. Takeda, G. Soda, and H. Chihara, *Solid State Commun.*, **36**, 445 (1980).
4) Y. Yoshimoto, T. Fujiwara, T. Atake, and H. Chihara, *Chem. Lett.*, **1985**, 1347.
5) T. Fujiwara, unpublished results.
6) S. Takeda, T. Fujiwara, and H. Chihara, *J. Phys. Soc. Jpn.*, **58**, 1793 (1989).
7) N. Yasuoka, private communication.
8) K. Saito, T. Atake, and H. Chihara, *J. Chem. Thermodyn.*, **19**, 633 (1987).
9) W. A. Johnson and R. F. Mehl, *Trans. Am. Inst. Min. Metall. Pet. Eng.*, **135**, 416 (1977).
10) C. N. R. Rao and K. J. Rao, "Phase Transitions in Solids," Chap. 4, McGraw-Hill (1978).